Figure S1

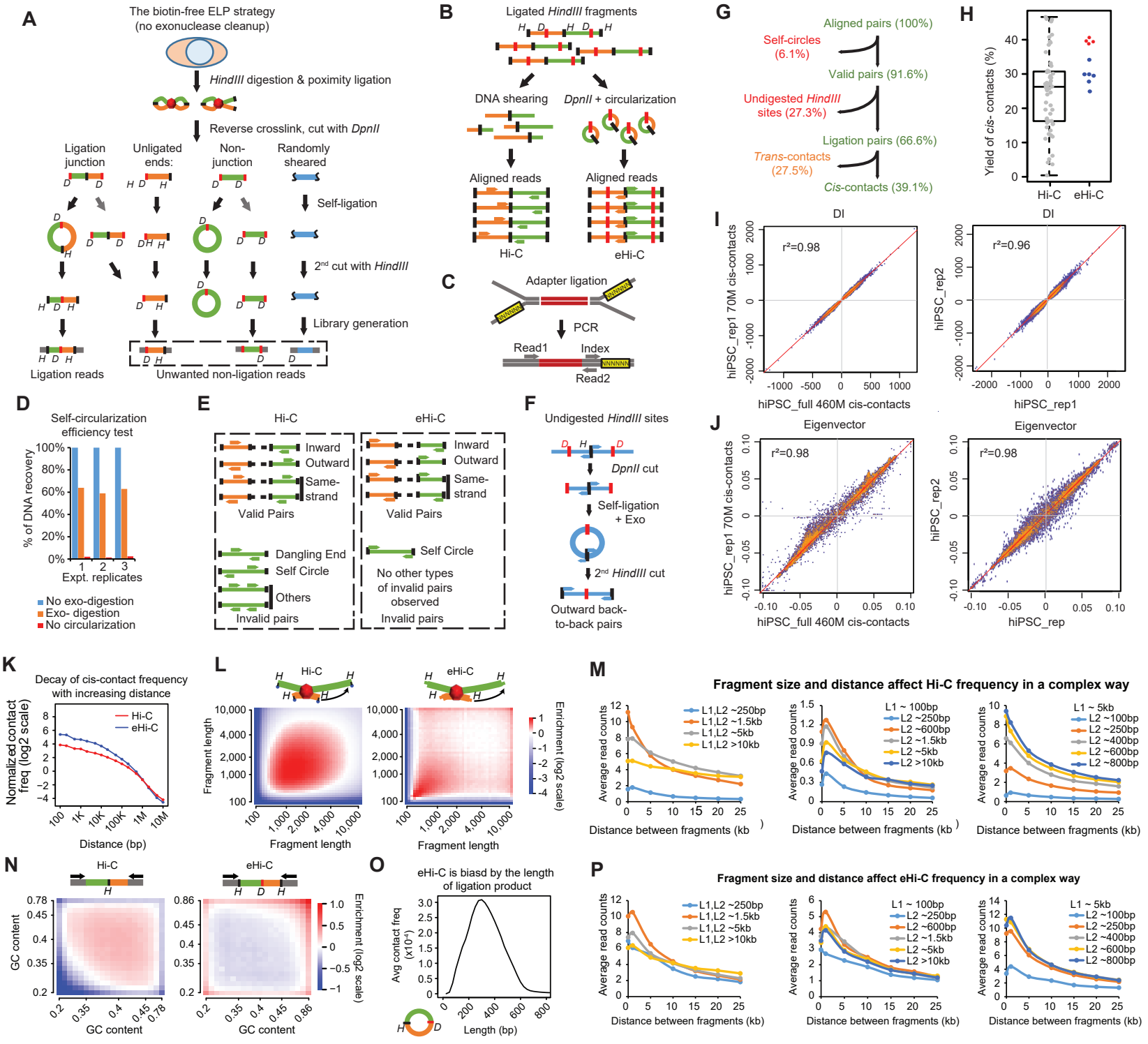
A
The biotin-free ELP strategy
(no exonuclease cleanup)
HindIII digestion & poximity ligation
Reverse crosslink, cut with DpnII
Ligation junction
Unligated ends:
Non-junction
Randomly sheared
Self-ligation
2nd cut with HindIII
Library generation
Ligation reads
Unwanted non-ligation reads
B
Ligated HindIII fragments
DNA shearing
DpnII + circularization
Aligned reads
Hi-C
eHi-C
C
Adapter ligation
PCR
Read1
Index
Read2
G
Aligned pairs (100%)
Self-circles (6.1%)
Valid pairs (91.6%)
Undigested HindIII sites (27.3%)
Ligation pairs (66.6%)
Trans-contacts (27.5%)
Cis-contacts (39.1%)
H
Yield of cis- contacts (%)
Hi-C
eHi-C
I
DI
r²=0.98
hiPSC_rep1 70M cis-contacts
hiPSC_full 460M cis-contacts
r²=0.96
hiPSC_rep2
hiPSC_rep1
D
Self-circularization efficiency test
% of DNA recovery
Expt. replicates
No exo-digestion
Exo- digestion
No circularization
E
Hi-C
eHi-C
Inward
Outward
Same-strand
Valid Pairs
Dangling End
Self Circle
Others
Invalid pairs
Self Circle
No other types of invalid pairs observed
Invalid pairs
F
Undigested HindIII sites
DpnII cut
Self-ligation + Exo
2nd HindIII cut
Outward back-to-back pairs
J
Eigenvector
r²=0.98
hiPSC_rep1 70M cis-contacts
hiPSC_full 460M cis-contacts
hiPSC_rep2
hiPSC_rep
K
Decay of cis-contact frequency with increasing distance
Normalized contact freq (log2 scale)
Hi-C
eHi-C
Distance (bp)
L
Hi-C
eHi-C
Fragment length
Enrichment (log2 scale)
M
Fragment size and distance affect Hi-C frequency in a complex way
Average read counts
L1,L2 ~250bp
L1,L2 ~1.5kb
L1,L2 ~5kb
L1,L2 >10kb
Distance between fragments (kb)
L1 ~ 100bp
L2 ~250bp
L2 ~600bp
L2 ~1.5kb
L2 ~5kb
L2 >10kb
L1 ~ 5kb
L2 ~100bp
L2 ~250bp
L2 ~400bp
L2 ~600bp
L2 ~800bp
N
Hi-C
eHi-C
GC content
Enrichment (log2 scale)
O
eHi-C is biasd by the length of ligation product
Avg contact freq (x10⁻⁴)
Length (bp)
P
Fragment size and distance affect eHi-C frequency in a complex way

Figure S1. Related to Figure 1 and STAR methods. Source of errors from eHi-C protocol and systematical biases in eHi-C experiments.

A, The scheme shows the different types of unwanted non-ligation reads (in dashed box) when the exonuclease cleanup step is omitted from eHi-C protocol (which is equivalent to the previously published ELP method (Tanizawa et al., 2010)). All these non-ligation reads can be effectively removed by exonuclease cleanup. **B**, For reproducible ligation DNA products between the same HindIII ends, (Left) Hi-C will generate different paired-end reads due to random DNA shearing. (Right) In eHi-C, these ligation events will form the same DNA circles, resulting in identical paired-end reads. **C**, We used a custom adapter with 6 random bases as a unique molecule index (UMI) to distinguish PCR duplicates. **D**, Test the efficiency of self-ligation. Naked genomic DNA were first digested with DpnII. Self-ligation reactions (2.5μg DNA in 1mL to mimic the eHi-C condition) were then performed before λ-exonuclease treatment. The efficiency of self-ligation was measured by the percentage of remaining DNA after exonuclease digestion (orange). No exonuclease controls are set at 100% (blue). DNA with no self-ligation step are completely digested (red). Results from 3 independent assays are shown. **E**, Valid Hi-C or eHi-C reads involve two *HindIII* fragments can be further classified based on strand orientation. The invalid Hi-C reads include “dangling end”, “self-circle” and “others” based on strand orientation, while the only type of invalid eHi-C reads is self-circles (right). **F**, Undigested HindIII sites are one major source of errors in eHi-C, which are read pairs mapped back-to-back at the same HindIII site. **G**, Data filtering results of one exemplary eHi-C library generated from 0.1M cells. **H**, Compare the yield of *cis*-contact reads between 57 published Hi-C libraries and 10 eHi-C libraries. The 4 red spots are eHi-C libraries prepared under *in situ* ligation condition. **I**, Left: comparison of Directionality Index (DI) of the full hiPSC data (6 replicates, 460M *cis*-contacts) and data from one replicate 70M (*cis*-Contacts). Right: comparison of DI from data of two hiPSC biological replicates. **J**, Left: comparison of PC1 values (equivalent to eigenvector) of the full hiPSC data and one replicate. Right: comparison of PC1 values of two hiPSC biological replicates. **K**, Curves showing the decay of *cis*-contact with an increasing distance between two *HindIII* restrictive fragments. Only “same-strand” reads (see **STAR Methods**) were used to plot the curves. **L**, Compare the bias from *HindIII* fragment length in Hi-C (left) and eHi-C (right) libraries. All the fragments are binned into 40 equal-sized groups, and the enrichment of *trans* reads between any two groups are plotted as heatmaps. The enrichment value is the ratio between actual read counts and the global average for any two groups. **M**, Curves plot how the distance decay profile changes when the length of *HindIII* fragments are different in H1 hESC Hi-C data. **N**, *HindIII* ends are binned into 20 groups based on GC content, and the enrichment of *trans*- reads are also plotted as heatmaps. For Hi-C (left) we used the GC content in the 200bp region upstream the *HindIII* site, and for eHi-C, we used the GC content of the region between the *HindIII* and its nearest *DpnII* site. **O**, Curve shows the average contact frequency from eHi-C against the length of ligation junction products forming DNA circles. **P**, The same analyses as **M** are performed with iPSC eHi-C data.

Figure S2

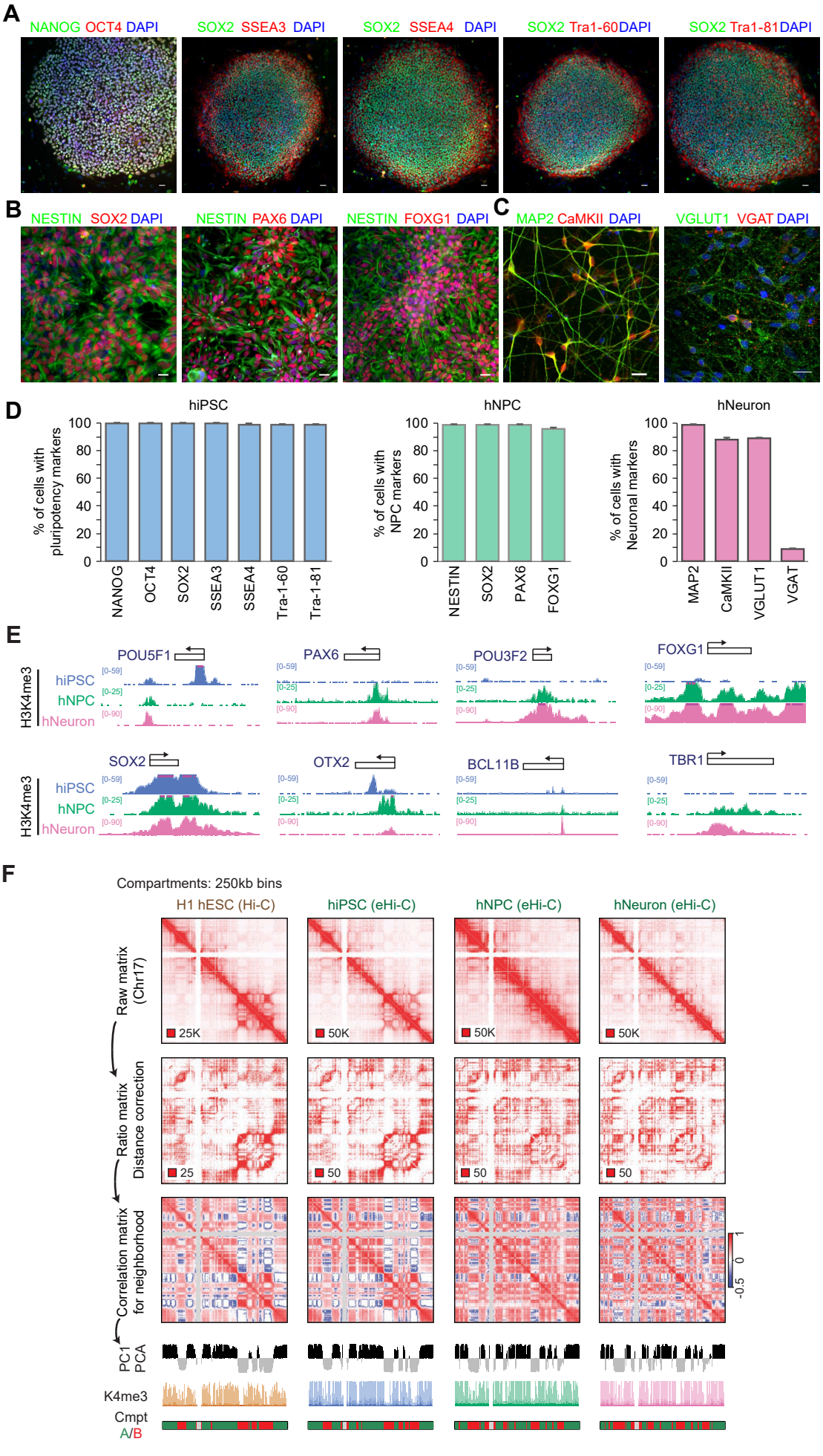
A
NANOG OCT4 DAPI
SOX2 SSEA3 DAPI
SOX2 SSEA4 DAPI
SOX2 Tra1-60DAPI
SOX2 Tra1-81DAPI
B
NESTIN SOX2 DAPI
NESTIN PAX6 DAPI
NESTIN FOXG1 DAPI
C
MAP2 CaMKII DAPI
VGLUT1 VGAT DAPI
D
hiPSC
% of cells with pluripotency markers
NANOG
OCT4
SOX2
SSEA3
SSEA4
Tra-1-60
Tra-1-81
hNPC
% of cells with NPC markers
NESTIN
SOX2
PAX6
FOXG1
hNeuron
% of cells with Neuronal markers
MAP2
CaMKII
VGLUT1
VGAT
E
H3K4me3
hiPSC
hNPC
hNeuron
POU5F1
PAX6
POU3F2
FOXG1
SOX2
OTX2
BCL11B
TBR1
F
Compartments: 250kb bins
H1 hESC (Hi-C)
hiPSC (eHi-C)
hNPC (eHi-C)
hNeuron (eHi-C)
Raw matrix (Chr17)
Ratio matrix Distance correction
Correlation matrix for neighborhood
PC1 PCA
K4me3
Cmpt A/B

Figure S2. Related to Figure 1 and STAR Methods. Characterization of forebrain-specific neural differentiation and Hi-C analysis at compartment level.
A, Confocal images of pluripotency marker immunostaining of hiPSCs. **B**, Confocal images of neural progenitor marker immunostaining of hNPCs. **C**, Confocal images of immunostaining of MAP2AB, CAMKII, VGLUT1 and VGAT. Scale bars, 20 μm. **D**, Quantification of cells with pluripotency, NPC and neuronal markers from fluorescent images. Values represent mean+/- SEM. **E**, H3K4me3 ChIPmentation results at representative marker genes. **F**, Compartment level comparison of Hi-C or eHi-C data at 250kb resolution. Correlation matrices were created after two steps of data transformations showing the 3D genome neighborhood; PC1 from principal component analysis (PCA) were used to call compartment A/B.

Figure S3

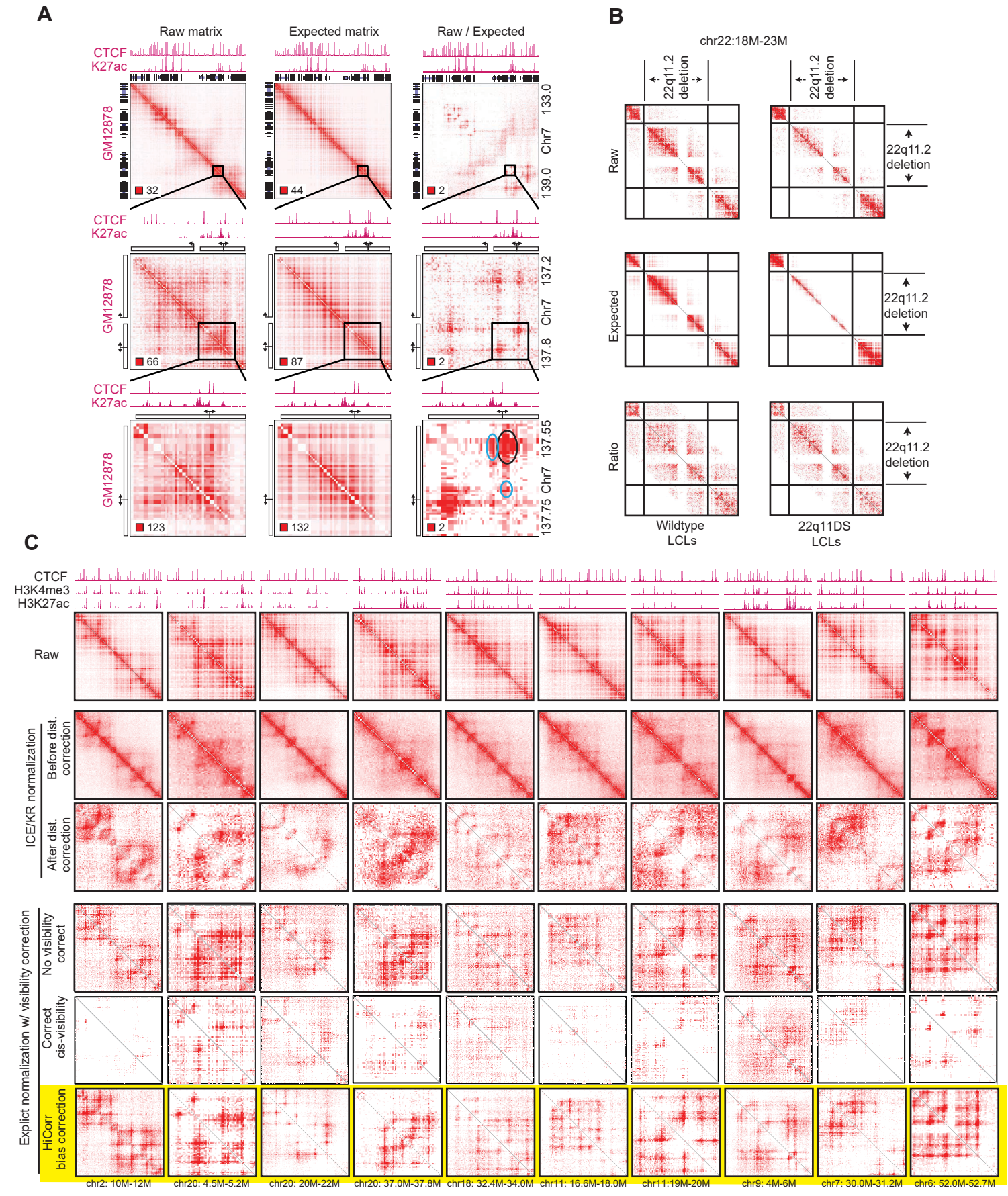
A
Raw matrix
Expected matrix
Raw / Expected
CTCF
K27ac
GM12878
32
44
2
133.0
Chr7
139.0
66
87
137.2
137.8
123
132
137.55
137.75
B
chr22:18M-23M
22q11.2 deletion
Raw
Expected
Ratio
Wildtype LCLs
22q11DS LCLs
C
CTCF
H3K4me3
H3K27ac
Raw
ICE/KR normalization
Before dist. correction
After dist. correction
Explict normalization w/ visibility correction
No visibility correct
Correct cis-visibility
HiCorr bias correction
chr2: 10M-12M
chr20: 4.5M-5.2M
chr20: 20M-22M
chr20: 37.0M-37.8M
chr18: 32.4M-34.0M
chr11: 16.6M-18.0M
chr11:19M-20M
chr9: 4M-6M
chr7: 30.0M-31.2M
chr6: 52.0M-52.7M

Figure S3. Related to Figure 2 and STAR methods. Hi-C analysis at loop levels, and more examples of HiCorr-correction.

A, Hi-C analysis at chromatin loop level. Raw, expected and ratio heatmaps in GM12878 cells at different zooming scales. Note that chromatin loop is only obvious in the ratio heatmaps. **B**, *HiCorr* can properly normalize copy number changes. Published Hi-C data (Zhang et al., 2018) in 6 wildtype LCLs (left column heatmaps) and 5 LCLs from 22q11 deletion syndrome patients (22q11DS, right column heatmaps) were pooled together for *HiCorr*-correction. All 22q11DS LCLs have heterozygous 22q11.2 deletion at the indicated location of the heatmap. As expected, raw heatmap from 22q11DS LCLs is weaker in the deletion region than outside the deletion region (because there is only one copy of genome). It should be noted that Zhang et al. compared the "normalized" heatmaps generated by a few Hi-C analysis pipelines, expecting weaker signal at the deletion region. Since *HiCorr* does not output "normalized" heatmaps, the copy number difference will be recognized as a bias in the "expected" heatmaps. The final ratio heatmaps will show no differences within the CNVs. This is an advantage because if there is a loop within the large CNV region, calling the loop from ratio heatmaps will not be affected. **C**, Examples comparing the heatmaps generated by various bias-correction strategies in GM12878 cells. Row 1: raw heatmaps at 10 loci. Comparing *HiCorr* (row 6) to other methods, we can tell that: (i) ICE/KR does not correct distance bias (row 2); (ii) *HiCorr* results are sharper and cleaner than ICE/KR + distance correction (row 3); (iii) explicit methods without visibility correction (row 4) has higher background; (iv) correcting cis-visibility (row 5) tends to cause over-correction.

Figure S4

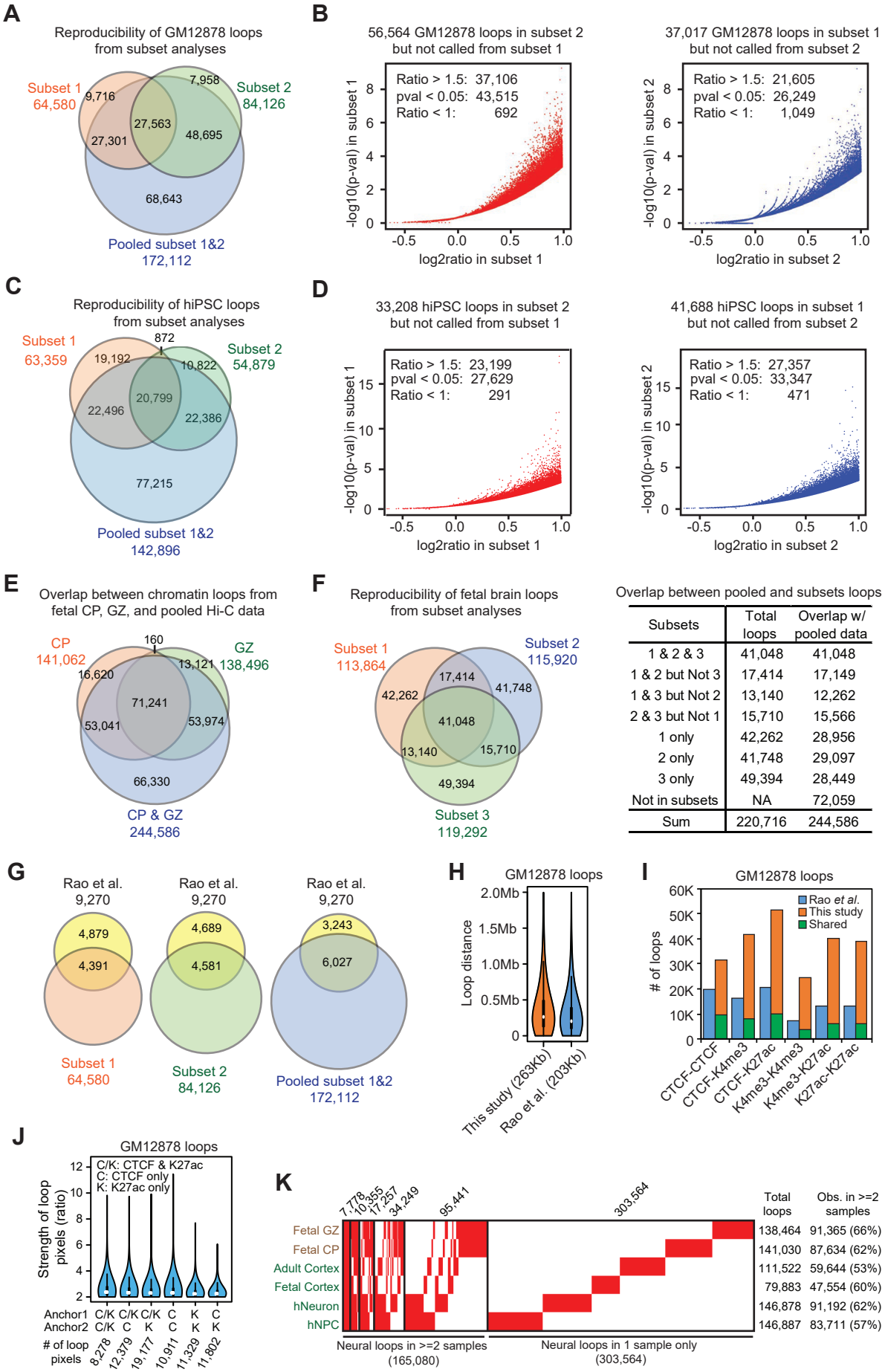
A
Reproducibility of GM12878 loops from subset analyses
Subset 1 64,580
Subset 2 84,126
9,716
7,958
27,563
48,695
27,301
68,643
Pooled subset 1&2 172,112
B
56,564 GM12878 loops in subset 2 but not called from subset 1
Ratio > 1.5: 37,106
pval < 0.05: 43,515
Ratio < 1: 692
-log10(p-val) in subset 1
log2ratio in subset 1
37,017 GM12878 loops in subset 1 but not called from subset 2
Ratio > 1.5: 21,605
pval < 0.05: 26,249
Ratio < 1: 1,049
-log10(p-val) in subset 2
log2ratio in subset 2
C
Reproducibility of hiPSC loops from subset analyses
Subset 1 63,359
Subset 2 54,879
872
19,192
10,822
20,799
22,496
22,386
77,215
Pooled subset 1&2 142,896
D
33,208 hiPSC loops in subset 2 but not called from subset 1
Ratio > 1.5: 23,199
pval < 0.05: 27,629
Ratio < 1: 291
41,688 hiPSC loops in subset 1 but not called from subset 2
Ratio > 1.5: 27,357
pval < 0.05: 33,347
Ratio < 1: 471
E
Overlap between chromatin loops from fetal CP, GZ, and pooled Hi-C data
CP 141,062
GZ 138,496
160
16,620
13,121
71,241
53,041
53,974
66,330
CP & GZ 244,586
F
Reproducibility of fetal brain loops from subset analyses
Subset 1 113,864
Subset 2 115,920
Subset 3 119,292
42,262
17,414
41,748
41,048
13,140
15,710
49,394
Overlap between pooled and subsets loops
Subsets | Total loops | Overlap w/ pooled data
1 & 2 & 3 | 41,048 | 41,048
1 & 2 but Not 3 | 17,414 | 17,149
1 & 3 but Not 2 | 13,140 | 12,262
2 & 3 but Not 1 | 15,710 | 15,566
1 only | 42,262 | 28,956
2 only | 41,748 | 29,097
3 only | 49,394 | 28,449
Not in subsets | NA | 72,059
Sum | 220,716 | 244,586
G
Rao et al. 9,270
Rao et al. 9,270
Rao et al. 9,270
4,879
4,391
4,689
4,581
3,243
6,027
Subset 1 64,580
Subset 2 84,126
Pooled subset 1&2 172,112
H
GM12878 loops
Loop distance
2.0Mb
1.5Mb
1.0Mb
0.5Mb
This study (263Kb)
Rao et al. (203Kb)
I
GM12878 loops
# of loops
Rao et al.
This study
Shared
CTCF-CTCF
CTCF-K4me3
CTCF-K27ac
K4me3-K4me3
K4me3-K27ac
K27ac-K27ac
J
GM12878 loops
C/K: CTCF & K27ac
C: CTCF only
K: K27ac only
Strength of loop pixels (ratio)
Anchor1 C/K C/K C/K C K K C
Anchor2 C/K C K C C K K
# of loop pixels 8,278 12,379 19,177 10,911 11,329 11,802
K
7,778
10,355
17,257
34,249
95,441
303,564
Fetal GZ
Fetal CP
Adult Cortex
Fetal Cortex
hNeuron
hNPC
Total loops | Obs. in >=2 samples
138,464 | 91,365 (66%)
141,030 | 87,634 (62%)
111,522 | 59,644 (53%)
79,883 | 47,554 (60%)
146,878 | 91,192 (62%)
146,887 | 83,711 (57%)
Neural loops in >=2 samples (165,080)
Neural loops in 1 sample only (303,564)

Figure S4. Related to STAR Methods. Reproducibility of chromatin loop calls.

A, Venn diagram show the overlap of loop calls (ratio > 2 and p < 0.001, **STAR Method**) between two subsets of GM12878 data (involving different biological replicates from different labs, **Table S1**), and the pooled datasets. **B**, Left: For all 56,564 loop pixels called from subset 2 but not subset 1 GM12878 Hi-C data, the scatter plot show their ratios and p values in subset 1. The numbers in the plot show that a majority of these non-reproducible pixels might be called significant when more relaxed cutoffs (ratio > 1.5 or p < 0.05) were used; only 692 pixels (< 1%) completely lack signal enrichment (ratio < 1). Right: Scatter plot similar to left showing the results of nonreproducible loops in subset 1. **C-D**, Same analysis as in **A-B** except that the analysis was done in hiPSC eHi-C data. The hiPSC biological replicates used in subset analysis is listed in **Table S1**. **E**, The overlap between cortex CP and GZ loops, and the loops after pooling CP and GZ data together. Note CP and GZ are two very close cortex regions and the data are generated by the same lab (Won et al., 2016). **F**, Left: The overlap of loop calls after split the CP and GZ data into 3 subsets, each with 1 CP and 1 GZ replicate (**Table S1**). Right: The overlap between loops in the three-way subset analysis and loops called after pooling the CP and GZ data together. Note that the pooled datasets capture nearly all the reproducible loops from subset analyses. **G**, The performance of our loop calls (6-cutter Hi-C) in recovering the loops called by Rao *et al*. (4-cutter in situ Hi-C) in GM12878 cells. **H**, Compare the loop distance distribution of the loop calls by our method and Rao et al. in GM12878 cells. **I**, The overlap of our loop calls and Rao *et al*. in GM12878 cells on *cis*-regulatory elements. Note that we call loops in the format of pixels, while Rao *et al*. loops in the format of a circle area with center and radius. To reconcile this, we compared our loop pixels with all the pixels covered by the Rao *et al*. loop circle area. Blue boxes: all pixels from Rao *et al*. loop circle areas; green: shared pixels between our method and Rao *et al*.; orange: new pixels called only in this study. Comparing the orange and green boxes, the fold increases at H3K4me3 and H3K27ac marked regions (>5 fold) are much higher than at CTCF sites, suggesting that our method called more enhancer and promoter looping. **J**, Compare the strength of loop pixels in GM12878 cells occupied by CTCF or H3K27Ac. **K**, The overlap between loops from the 6 neural (e)Hi-C datasets. ~60% of loops from any neural dataset are reproduced by at least two samples. These are regarded as high confident neural loops in our analysis.

Figure S5

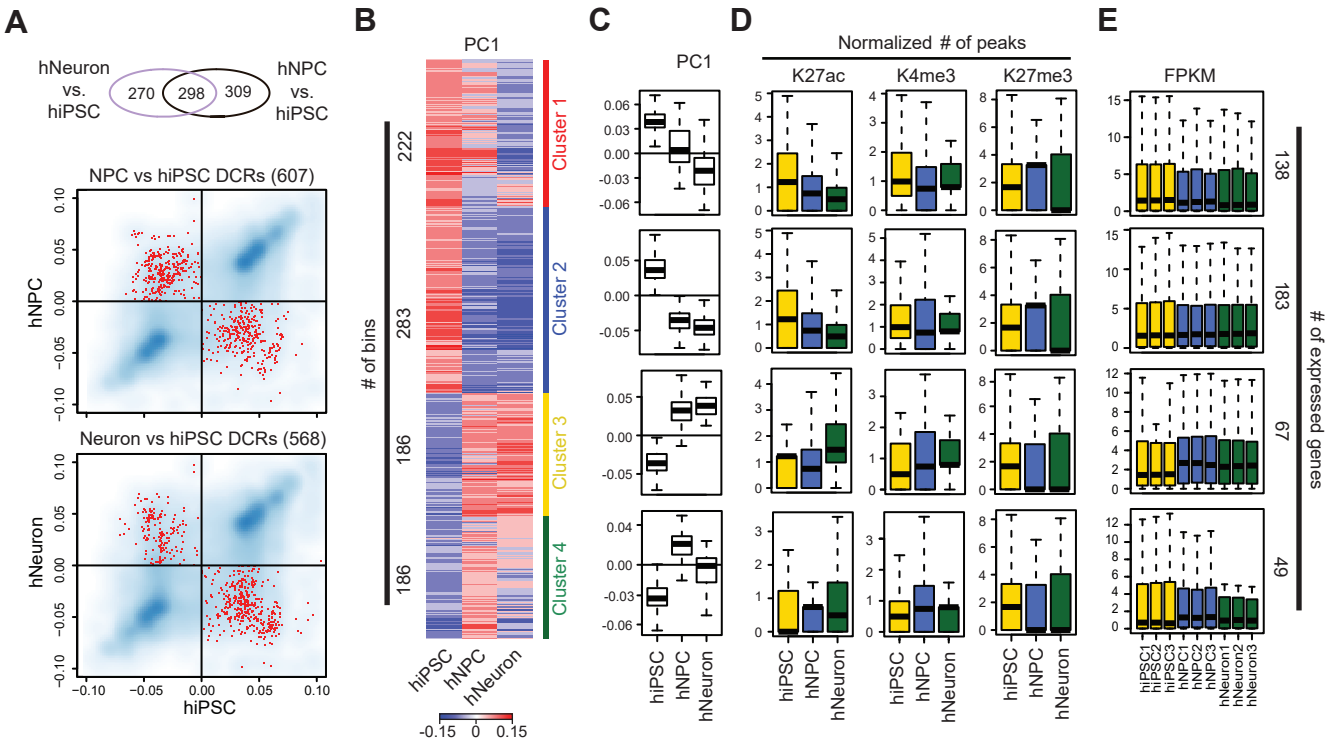

F

GO terms	P-value
Cluster 1 (537 genes)	
Carbohydrate binding	3.9E-08
Embryonic skeletal system morphogenesis	5.9E-07
Oxidoreductase activity	1.2E-05
Cluster 2 (667 genes)	
Intermediate filament	3.2E-06
Nucleic acid binding	8.6E-05
Ribonuclease activity	1.7E-04
Cluster 2 (276 genes)	
Methylation-dependent chromatin silencing	2.1E-04
nucleoside triphosphate biosynthetic process	3.4E-04
Cluster 4 (281 genes)	
Olfactory receptor activity	8.5E-22
G-protein coupled receptor activity	4.1E-19
Transmembrane signaling receptor activity	7.3E-11
Serine-type endopeptidase activity	9.2E-08
Integral component of membrane	9.8E-06

G

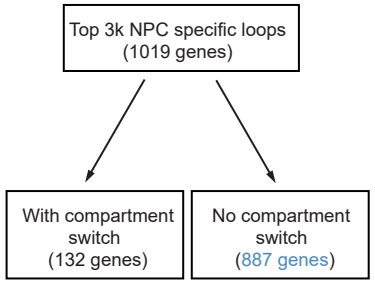

GO terms (887 non-switching genes)	P-value
Forebrain cell migration	2.2E-02
Regulation of nervous system development	2.4E-02
Regulation of neuron differentiation	2.8E-02
Morphogenesis involved in neuron differentiation	3.4E-02
Heart Morphogenesis	3.5E-02
Forbrain development	4.5E-02
Cerebral cortex development	4.9E-02

H

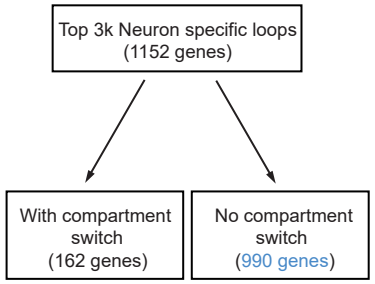

GO terms (990 non-switching genes)	P-value
Forebrain cell migration	3.5E-04
Cerebral cortex development	1.5E-03
Morphogenesis involved in neuron differentiation	7.1E-03
Central nervous system neuron differentiation	1.0E-02
Forbrain development	1.6E-02
Neuron migration	2.1E-02
Cell fate commitment	3.3E-02

Figure S5. Related to Figure 4. Genome compartment changes in neuronal differentiation. A, We called DCRs ($p < 0.05$, **STAR Methods**) in both hNPC and hNeuron comparing to hiPSCs, and only the DCRs switching their compartment were used in follow-up analyses. Upper: Venn diagram showing the overlap between DCRs in hNPC and hNeuron. Middle: Scatter plot comparing the PC1 values in hNPC and hiPSC cells. All bins in the genome were shown in the background as scatter cloud; red dots are the DCRs switching their compartment during the differentiation from hiPSC to hNPC cells. Lower: same as middle panel but comparing hNeuron to hiPSC. **B**, The 877 DCRs are classified into 4 clusters based on PC1 values representing different patterns of compartment switching. **C**, Box plots summarize the PC1 values of each DCR cluster. **D**, Box plots showing normalized numbers of histone mark peaks from DCRs in each cluster. **E**, Expression of corresponding genes in each cluster. **F**, GO analysis of genes in each DCR clusters. **G-H**, Gene ontology analysis of genes at hNPC-specific (**G**) and hNeuron-specific (**H**) loops but without compartment switching.

Figure S6

A

Chromatin loops at cis-regulatory elements

Chromatin loops	hiPSC	hNPC	hNeuron
w/ CTCF	11,406	15,233	22,001
w/ promoters	5,102	7,748	10,393
w/ enhancers	3,619	7,533	13,689

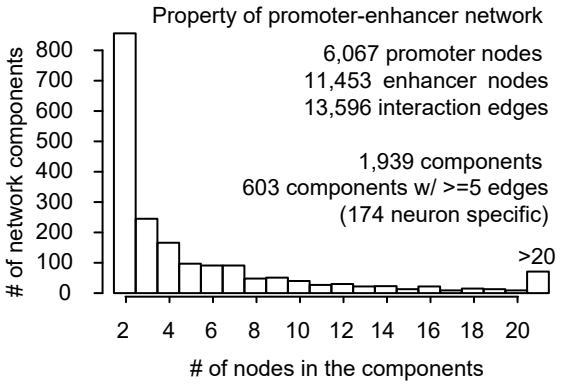

B

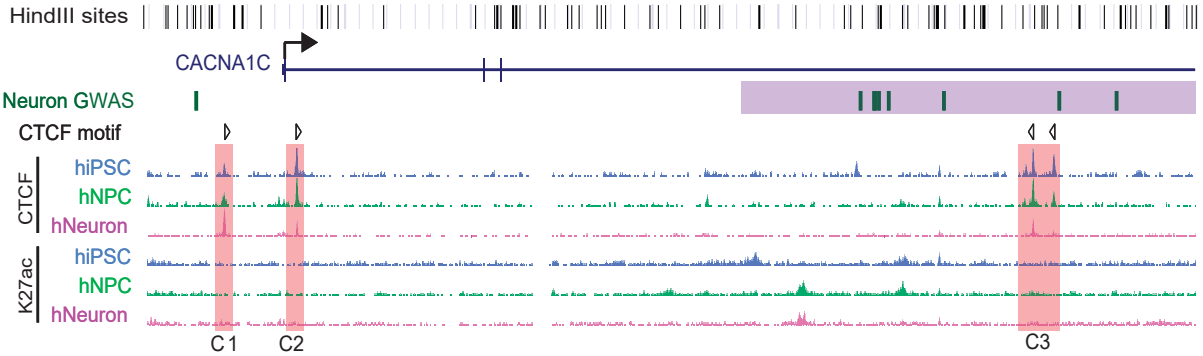

C

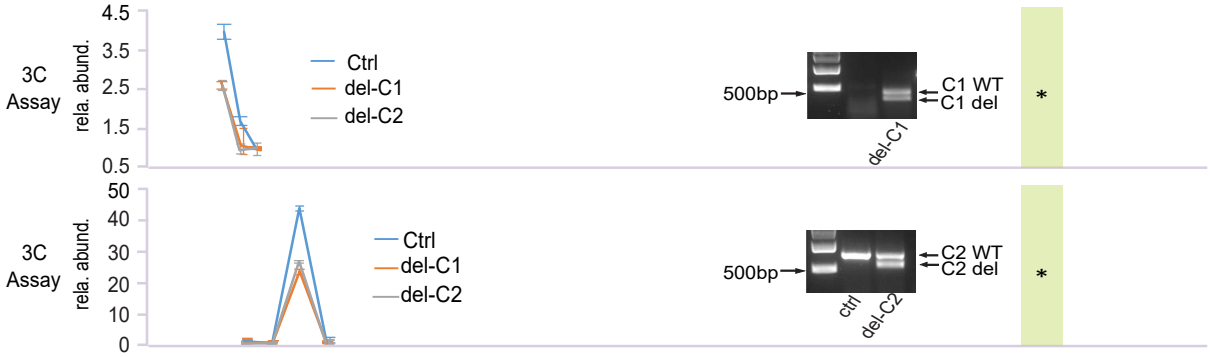

Figure S6. Related to Figure 5 and 6F-H. Enhancer aggregates in neural differentiation, and CTCF sites are responsible for the DNA loop at CACNA1C locus in hESC.
A, Left: Summary of chromatin loop numbers overlapping different types of *cis*-regulatory elements in neural differentiation. Right: Summary of components in our enhancer-promoter looping network analyses. **B**, Genomic features of *CACNA1C* locus. HindIII site track is shown as reference for 3C assays. C1, C2 and C3 are the CTCF sites with the motif direction shown above. **C**, 3C assays in H9 hESC cells. C1 and C2 sites were deleted respectively in H9 cells, and a nucleofection with no sgRNA was used as control. Deletion efficiency was shown as in the gel figures. 3C assay was done in three biological replicates. The relative PCR abundance was calculated to a nearby region which shows no interaction with C3 region from Hi-C. The anchor fragment is highlighted in yellow. Error bars: *s.d.* from the three replicates.

SUPPLEMENTAL DATA

Data S1: Additional Examples Relevant to Main Findings, Related to Figure 5 and 6.

Data S1, I. Related to Figure 5. Enhancer aggregates in neural differentiation.

A-I, Examples that gain chromatin loops during neural differentiation; heatmaps in hiPSC, hNPC, hNeuron and fetal CP are shown. **J**, RNA-seq expression data of key neural genes in these regions, including *FOXG1* gene shown in **Figure 5B**. Genes in red are upregulated and in green are downregulated.

Data S1, II. Related to Figure 5D-F. Genes in neural enhancer aggregates can be both up- and downregulated in neural differentiation.

A-C, Example enhancer aggregate regions that involve many promoters and enhancers. Gene names in the aggregated region are listed on the left. **D**, RNA-seq data of the genes in these enhancer aggregations demonstrated the coordinated gene downregulation in example **A** and **B**, and coordinated gene upregulation in example **C**.

Data S1, III. Related to Figure 6C. Neural loops does not predict brain-specific genes for randomly chosen GWAS SNPs.

A, Results from two iterations of the same analysis as in **Fig. 6C**, except that we use randomly selected GWAS SNPs (after excluding brain GWAS SNPs). Briefly, for a random set of GWAS SNPs, we used neural loops to predict ~1,000 target genes, and compare their expression to eQTL predicted genes in 48 GTeX tissues. Tissue with red stars: neural loop predicted genes have higher expression levels than eQTL predicted genes. *p<1e-2,**p<1e-3,***p<1e-4,****p<1e-5; Highlighted in yellow: 13 brain tissues. **B**, Upper panel: a table shows how we compute a significance score (the -log10(pval) in fisher's exact test) indicating if brain tissues tend to get more significance stars (shown in **A**) than non-brain tissues. First row in red shows the score when using brain GWAS SNPs; the other rows are the scores from random iterations. Lower panel: the bias scores from 200 random iterations were summarized in a histogram and compared to the score from the analysis of brain GWAS SNPs (red arrow).

Data S1, IV. Related to Figure 6. Examples of several known neural disease risk loci.
For these examples, heatmaps of hiPSC, hNPC, hNeuron, fetal CP, fetal and adult cortex are shown to demonstrate the overall agreements between differentiated neurons and primary tissues. Note some examples gain new DNA contacts in differentiation, while some examples have preexisting DNA contacts.

Data S1, I

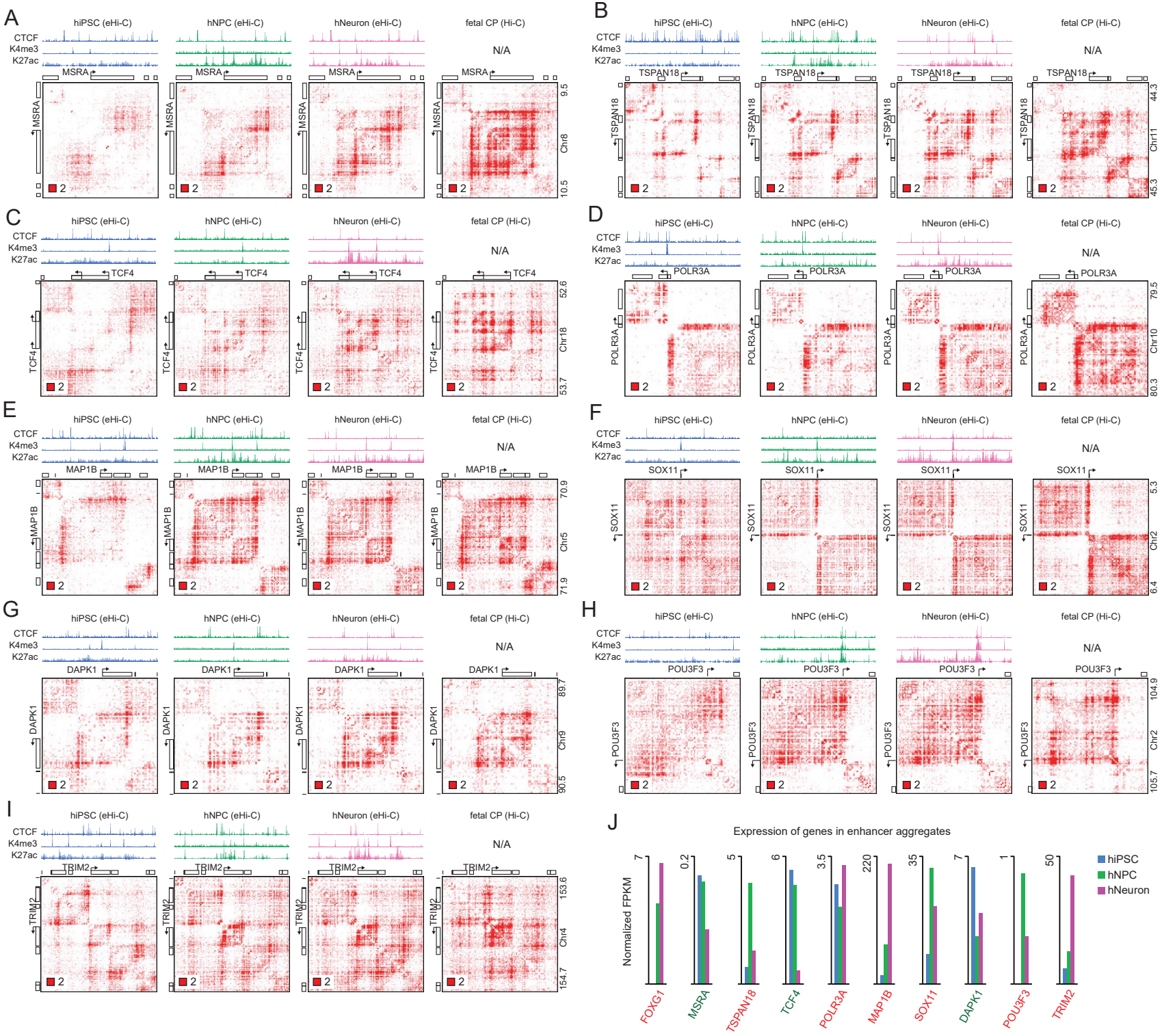
A
B
C
D
E
F
G
H
I
J
hiPSC (eHi-C)
hNPC (eHi-C)
hNeuron (eHi-C)
fetal CP (Hi-C)
CTCF
K4me3
K27ac
N/A
MSRA
TSPAN18
TCF4
POLR3A
MAP1B
SOX11
DAPK1
POU3F3
TRIM2
Chr8
Chr11
Chr18
Chr10
Chr5
Chr2
Chr9
Chr4
Expression of genes in enhancer aggregates
Normalized FPKM
hiPSC
hNPC
hNeuron
FOXG1
MSRA
TSPAN18
TCF4
POLR3A
MAP1B
SOX11
DAPK1
POU3F3
TRIM2

Data S1, II

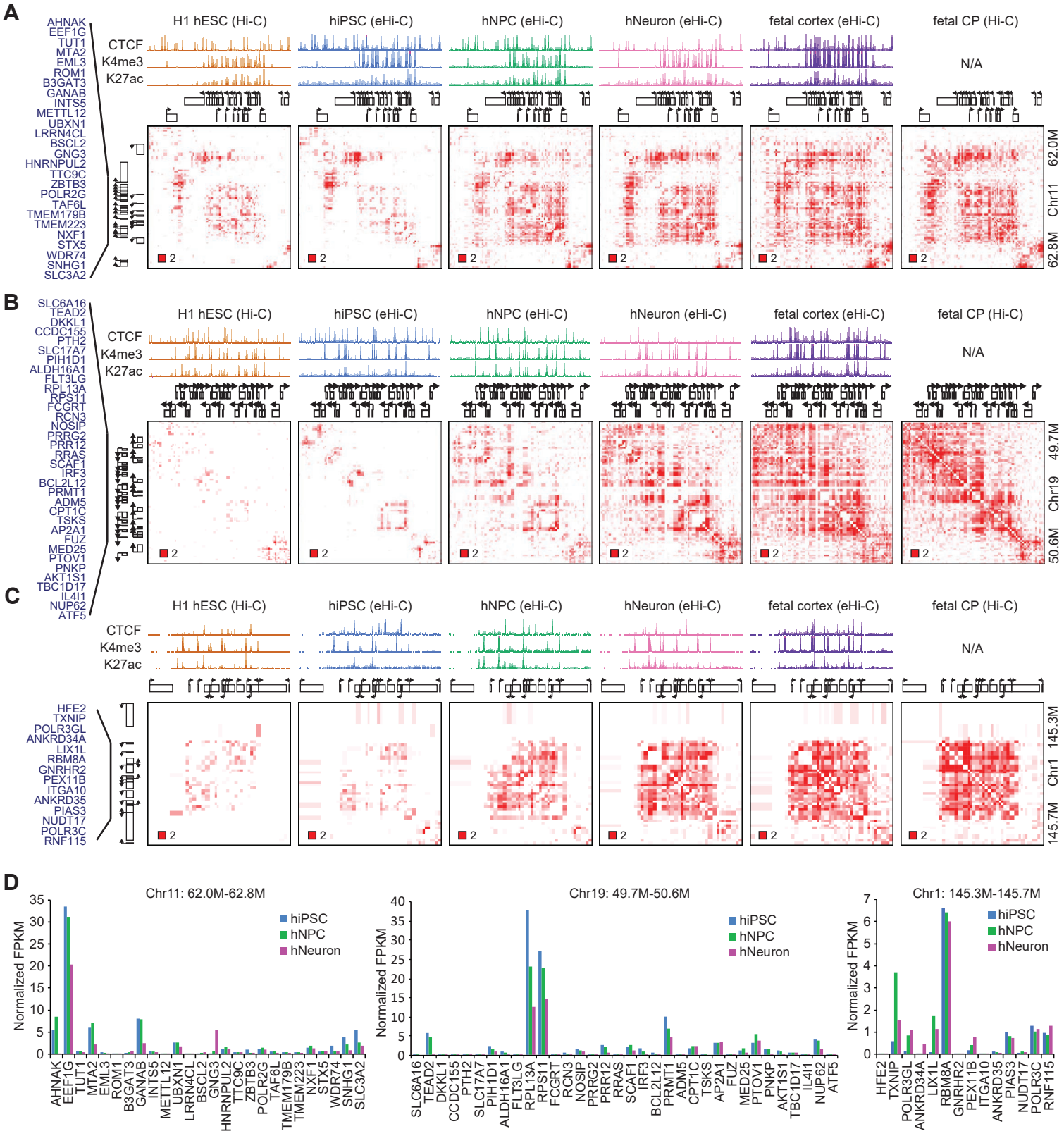
A
AHNAK
EEF1G
TUT1
MTA2
EML3
ROM1
B3GAT3
GANAB
INTS5
METTL12
UBXN1
LRRN4CL
BSCL2
GNG3
HNRNPUL2
TTC9C
ZBTB3
POLR2G
TAF6L
TMEM179B
TMEM223
NXF1
STX5
WDR74
SNHG1
SLC3A2
H1 hESC (Hi-C)
hiPSC (eHi-C)
hNPC (eHi-C)
hNeuron (eHi-C)
fetal cortex (eHi-C)
fetal CP (Hi-C)
CTCF
K4me3
K27ac
N/A
62.0M
Chr11
62.8M
B
SLC6A16
TEAD2
DKKL1
CCDC155
PTH2
SLC17A7
PIH1D1
ALDH16A1
FLT3LG
RPL13A
RPS11
FCGRT
RCN3
NOSIP
PRRG2
PRR12
RRAS
SCAF1
IRF3
BCL2L12
PRMT1
ADM5
CPT1C
TSKS
AP2A1
FUZ
MED25
PTOV1
PNKP
AKT1S1
TBC1D17
IL4I1
NUP62
ATF5
49.7M
Chr19
50.6M
C
HFE2
TXNIP
POLR3GL
ANKRD34A
LIX1L
RBM8A
GNRHR2
PEX11B
ITGA10
ANKRD35
PIAS3
NUDT17
POLR3C
RNF115
145.3M
Chr1
145.7M
D
Chr11: 62.0M-62.8M
Chr19: 49.7M-50.6M
Chr1: 145.3M-145.7M
Normalized FPKM
hiPSC
hNPC
hNeuron

Data S1, III

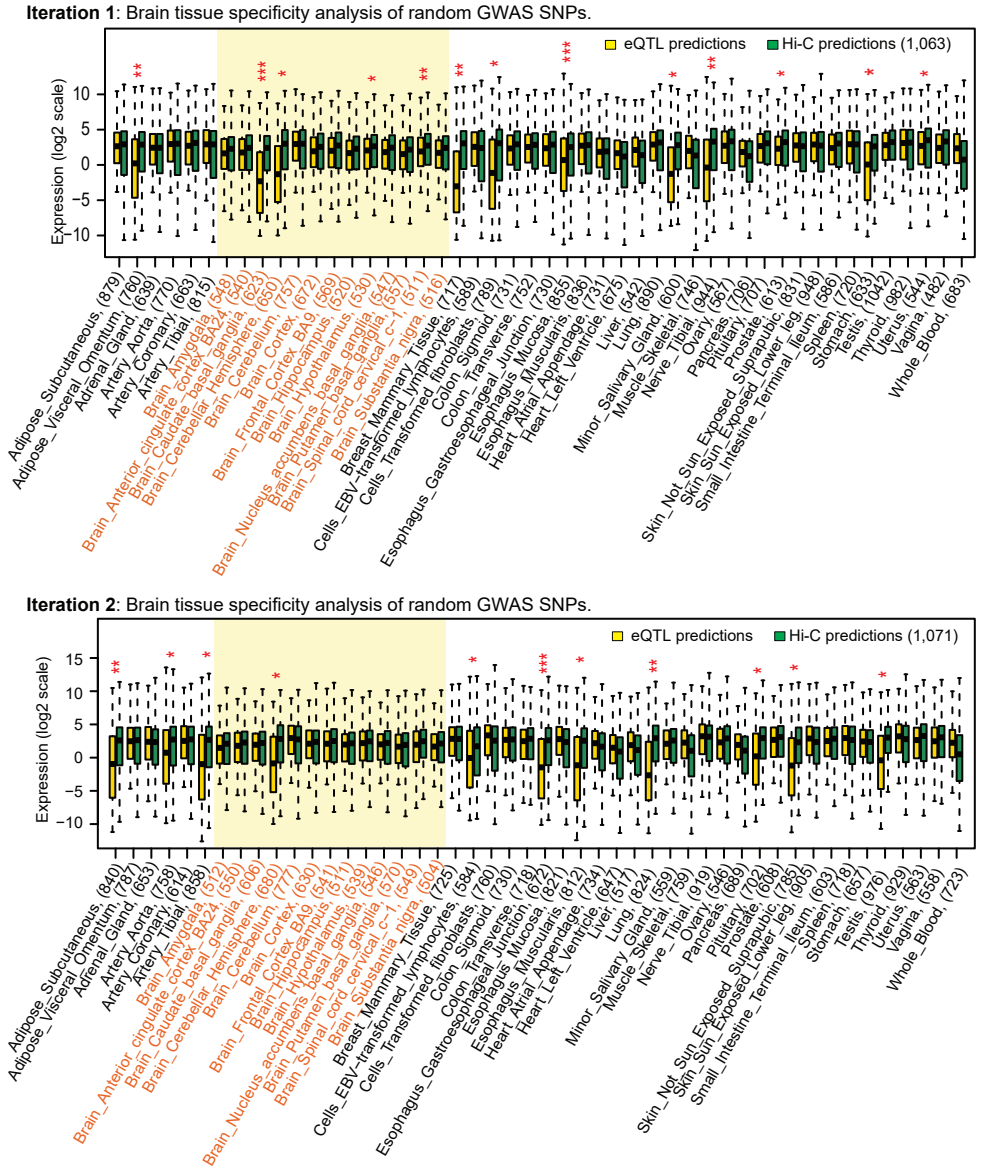

B

	# of brain tissues with a star (out of 13)	# of other tissues with a star (out of 35)	Score of brain tissue bias -log10(pval)
Brain GWAS SNPs	12	4	6.516
Iteration 1 random GWAS	4	9	0.138
Iteration 2 random GWAS	1	10	0.610
...	200 iterations		

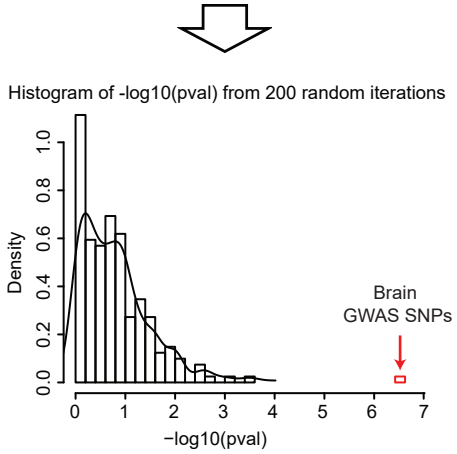

Data S1, IV

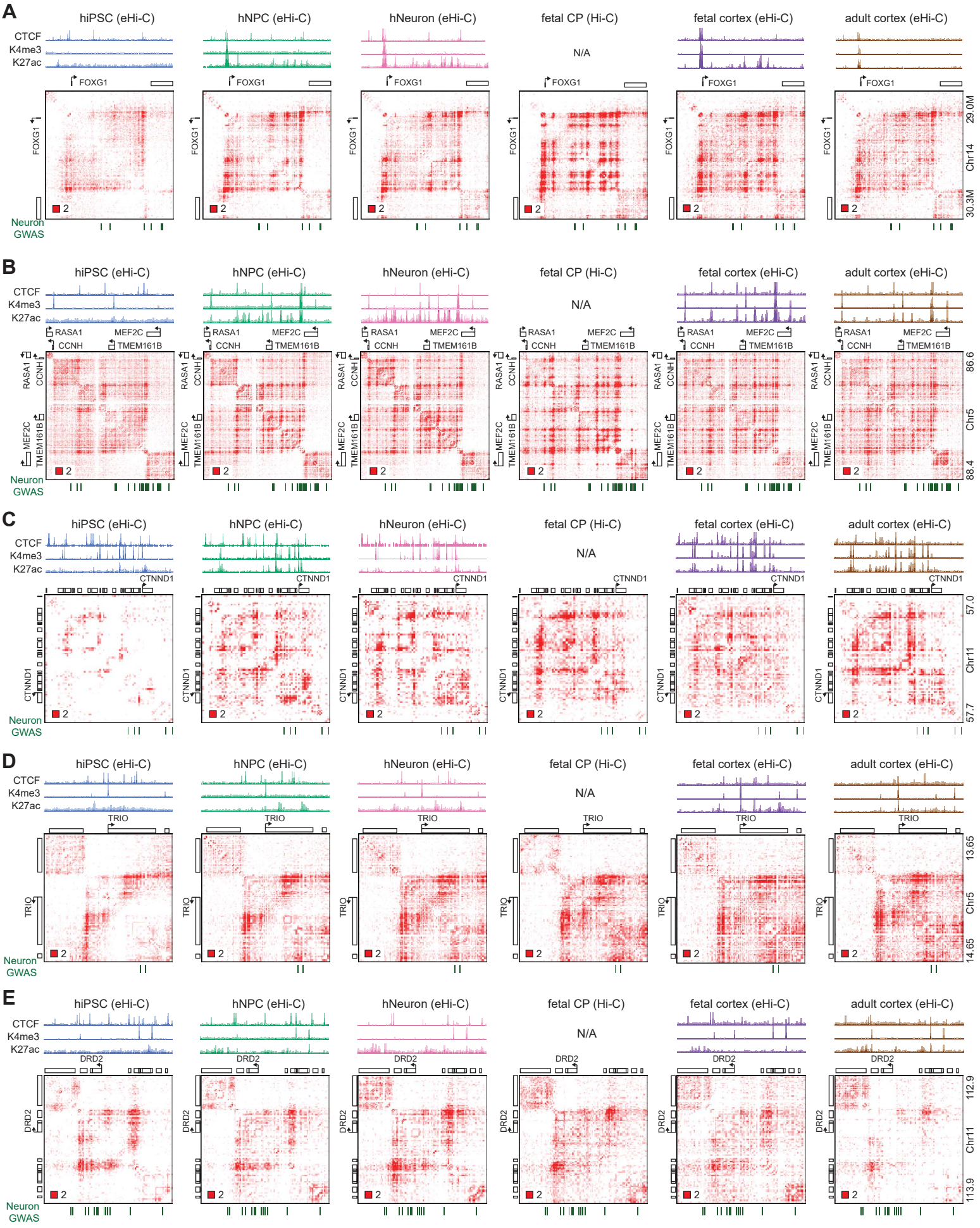
A
hiPSC (eHi-C)
hNPC (eHi-C)
hNeuron (eHi-C)
fetal CP (Hi-C)
fetal cortex (eHi-C)
adult cortex (eHi-C)
CTCF
K4me3
K27ac
N/A
FOXG1
Neuron GWAS
29.0M
Chr14
30.3M
B
RASA1
CCNH
MEF2C
TMEM161B
86.6
Chr5
88.4
C
CTNND1
57.0
Chr11
57.7
D
TRIO
13.65
Chr5
14.65
E
DRD2
112.9
Chr11
113.9